Supplementary data

Supplementary Information

Illumination-Boosted Capacitance with $NiFe_2O_4$: Design and Performance of Symmetric and Asymmetric Photo-powered Supercapacitors with Self-Generated Voltage

Shekoufeh Pira [a], Mohamad Mohsen Momeni [a*], Fuxiang Zhang [b]

[a] *Department of Chemistry, Isfahan University of Technology, Isfahan 84156-83111, Iran*

[b] *State Key Laboratory of Catalysis, Dalian Institute of Chemical Physics, Chinese Academy of Sciences, Dalian National Laboratory for Clean Energy. 116023 Dalian, P.R. China*

[*]Corresponding author. Email address : mm.momeni@cc.iut.ac.ir

Supplementary data

Synthesis of $NiFe_2O_4$

Nano ferrites are formed through the rapid precipitation of metal hydroxides, which subsequently transform into ferrites. In the initial stage, small solid hydroxide particles are generated by co-precipitating metal cations in an alkaline environment (the co-precipitation step), as depicted in following equations:[1]

$$Ni^{2+} + 2Fe^{2+} + 8OH^- \rightarrow Ni(OH)_2.2Fe(OH)_3\downarrow \quad (1)$$

During heating of the metal hydroxide solid solution in an alkaline medium, ferritization occurs, producing complex nickel ferrites.

$$Ni(OH)_2.2Fe(OH)_3 \rightarrow NiFe_2O_4 \,.\, n\mathrm{H2O} \quad (2)$$

Supplementary data

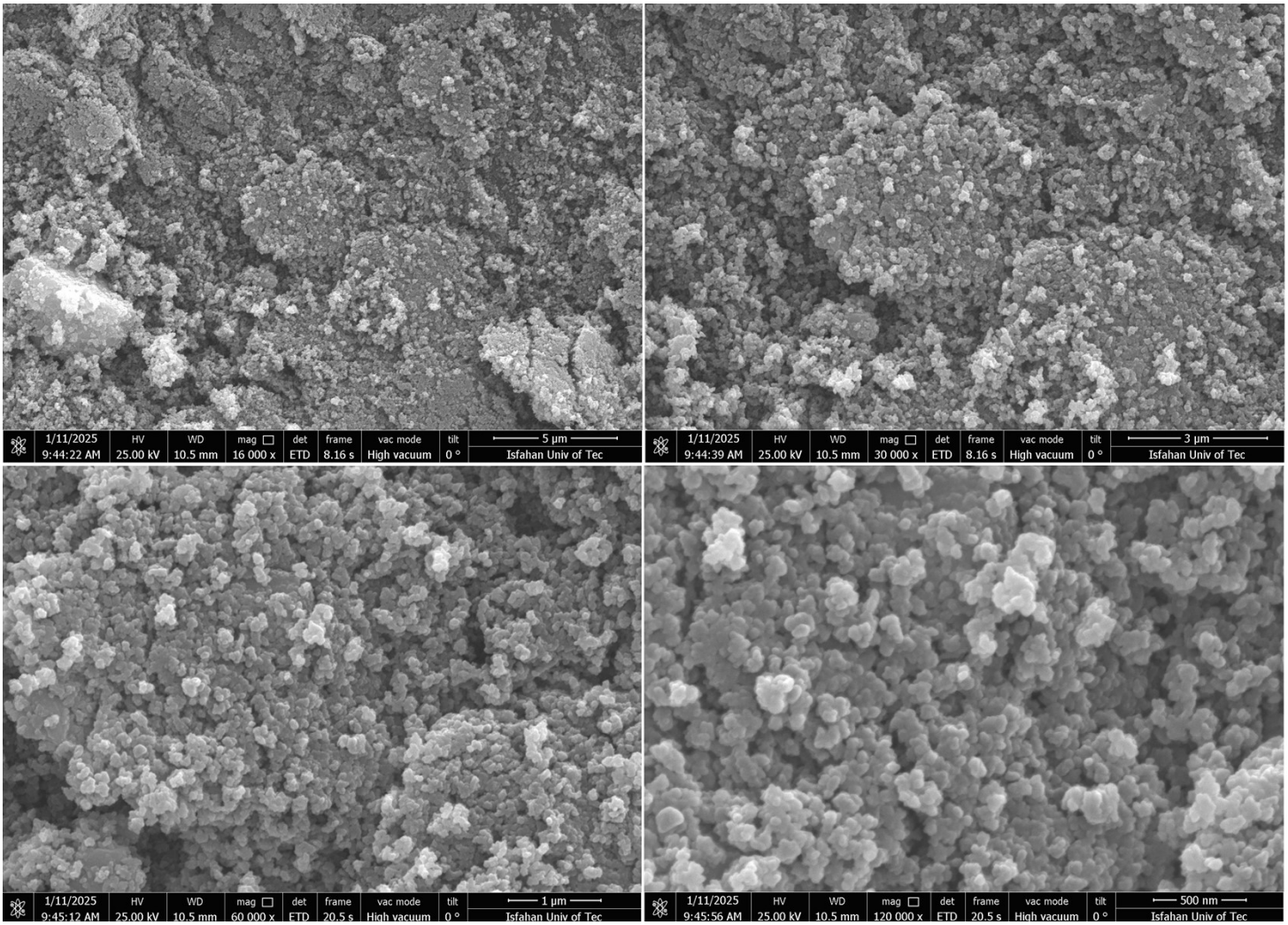

Fig. S1 SEM images, at different magnifications ×16000, ×30000, ×60000, and ×120000 of sample NF-400.

Supplementary data

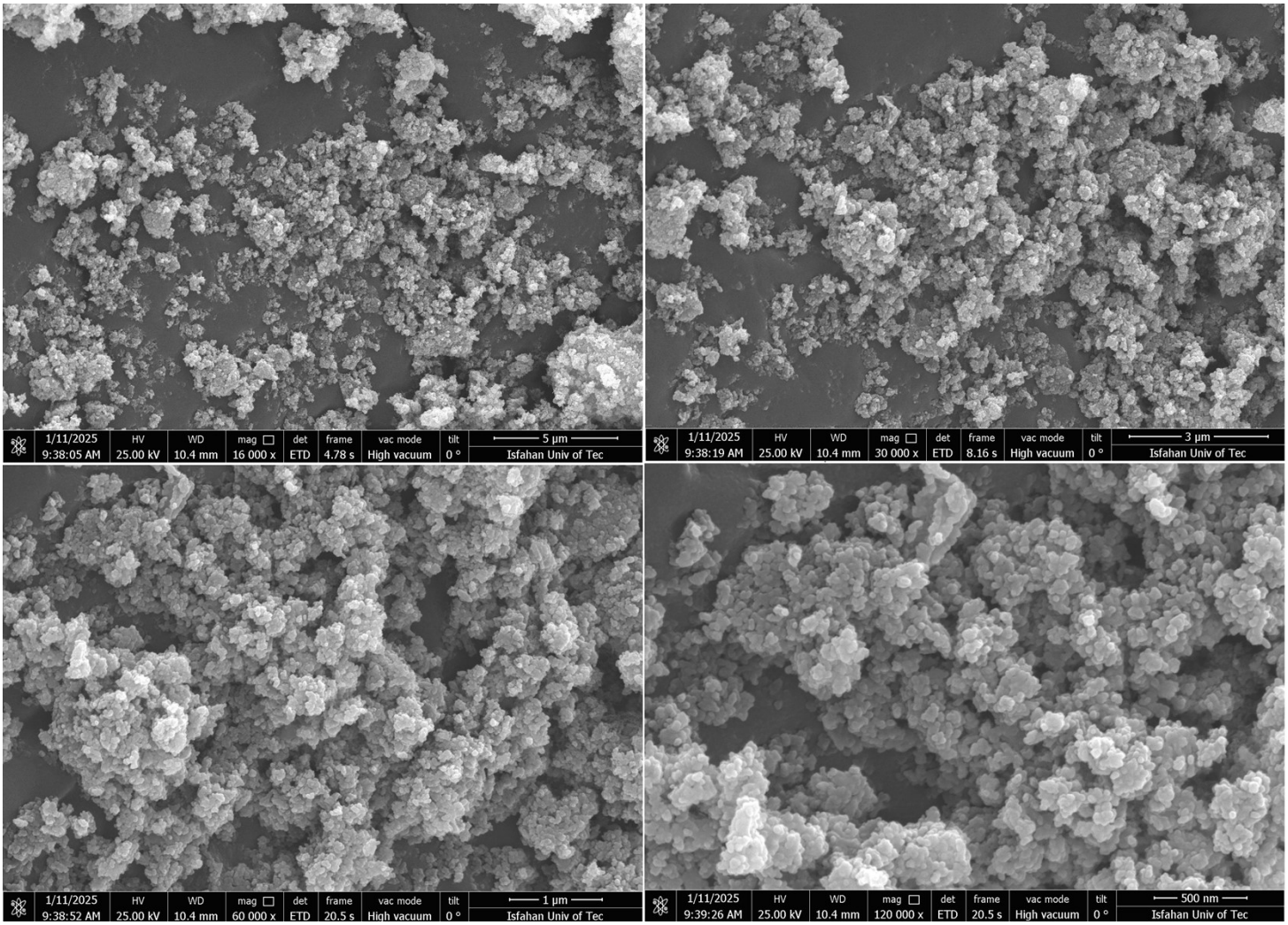

Fig. S2 SEM images, at different magnifications ×16000, ×30000, ×60000, and ×120000 of sample NF-500.

Supplementary data

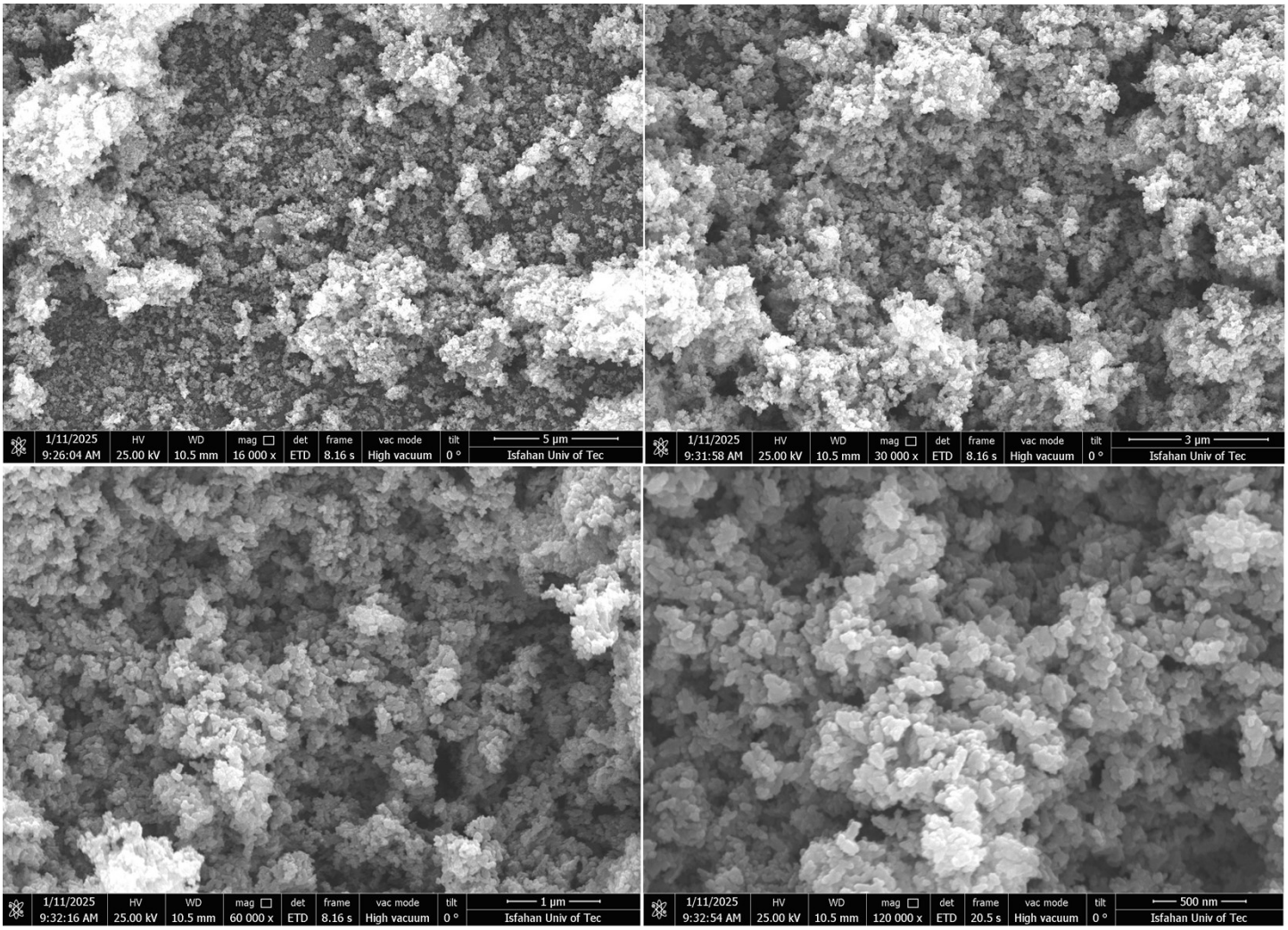

Fig. S3 SEM images, at different magnifications ×16000, ×30000, ×60000, and ×120000 of sample NF-600.

Supplementary data

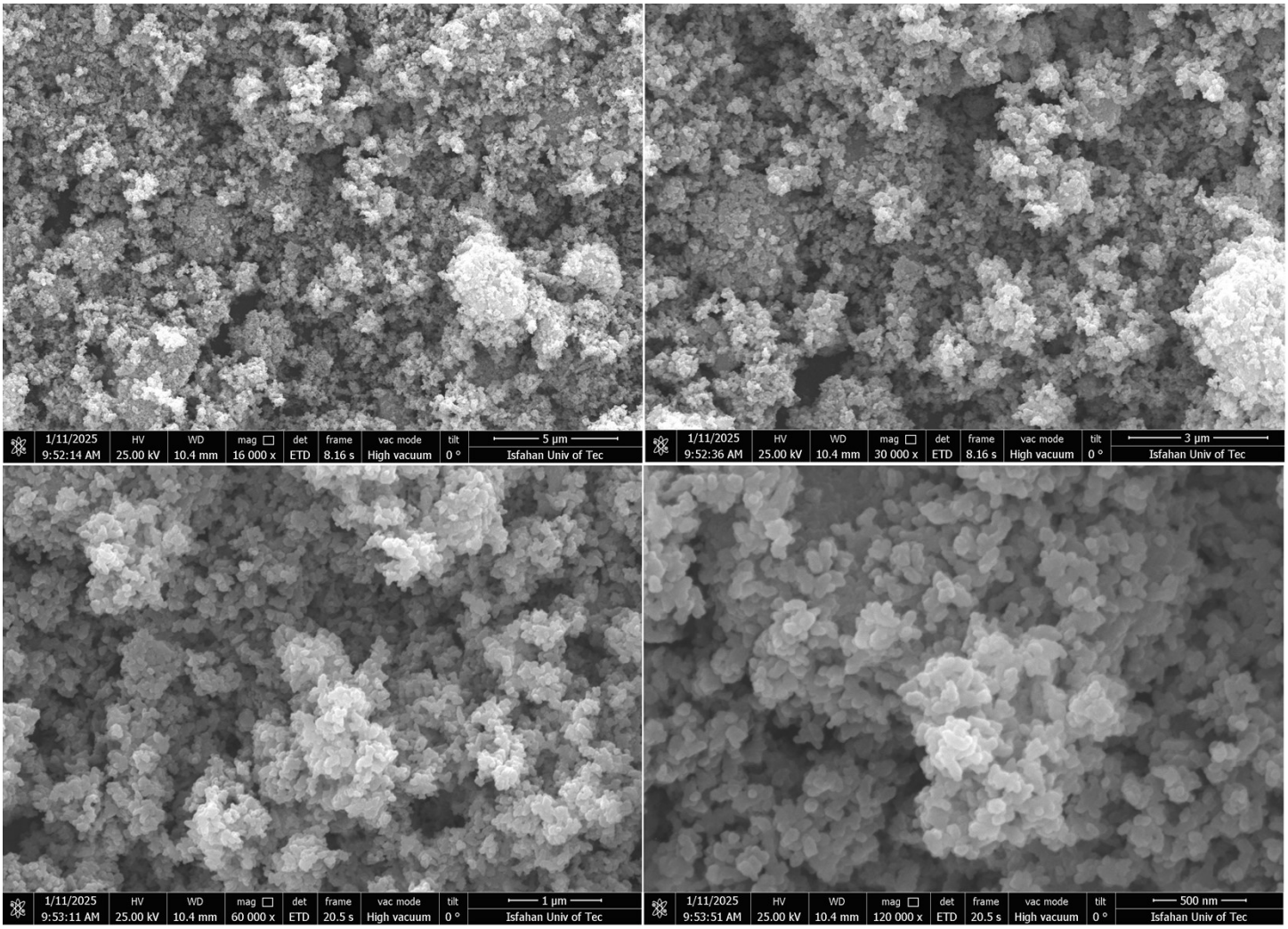

Fig. S4 SEM images, at different magnifications ×16000, ×30000, ×60000, and ×120000 of sample NF-700.

Supplementary data

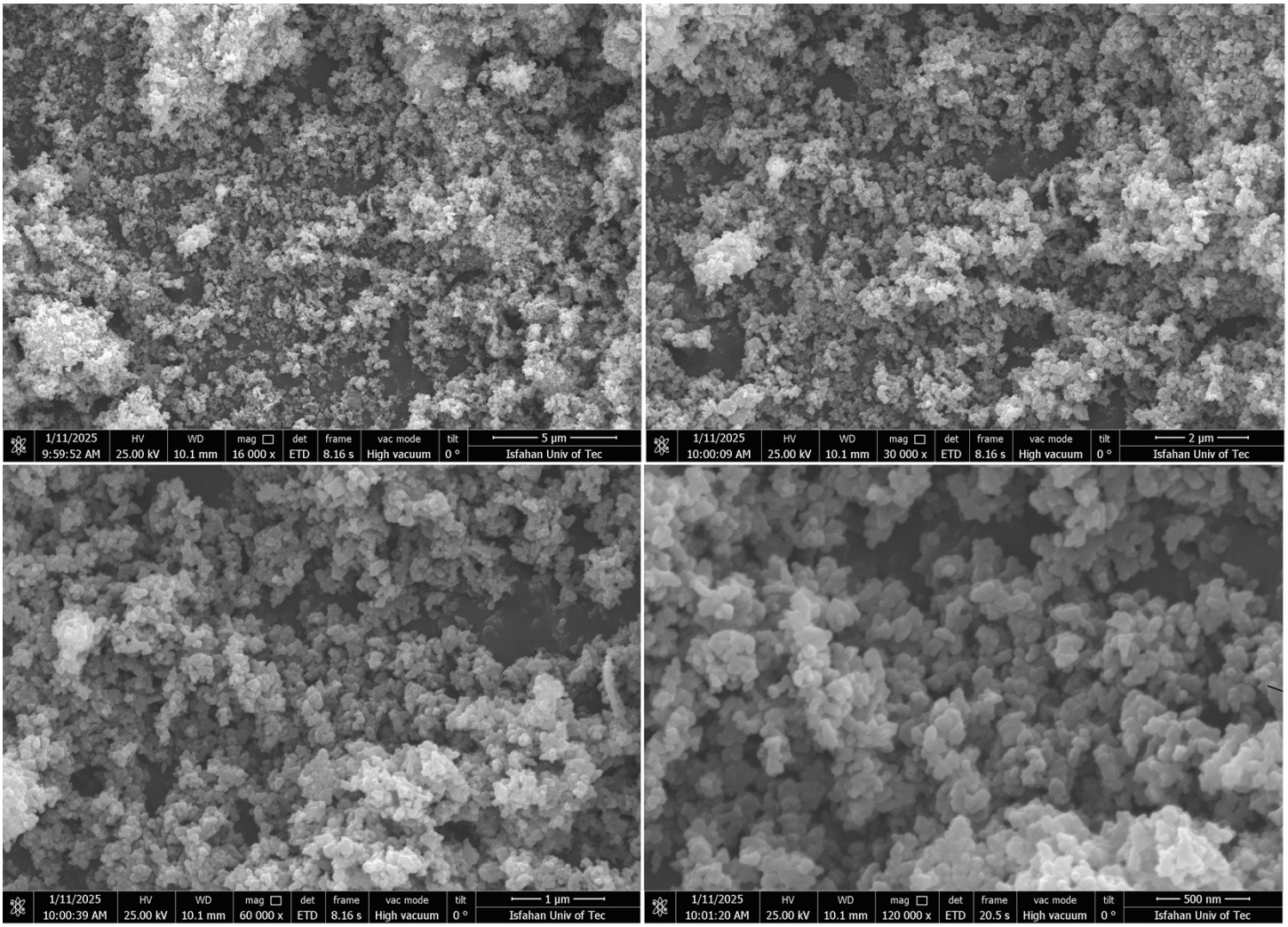

Fig. S5 SEM images, at different magnifications ×16000, ×30000, ×60000, and ×120000 of sample NF-800.

Supplementary data

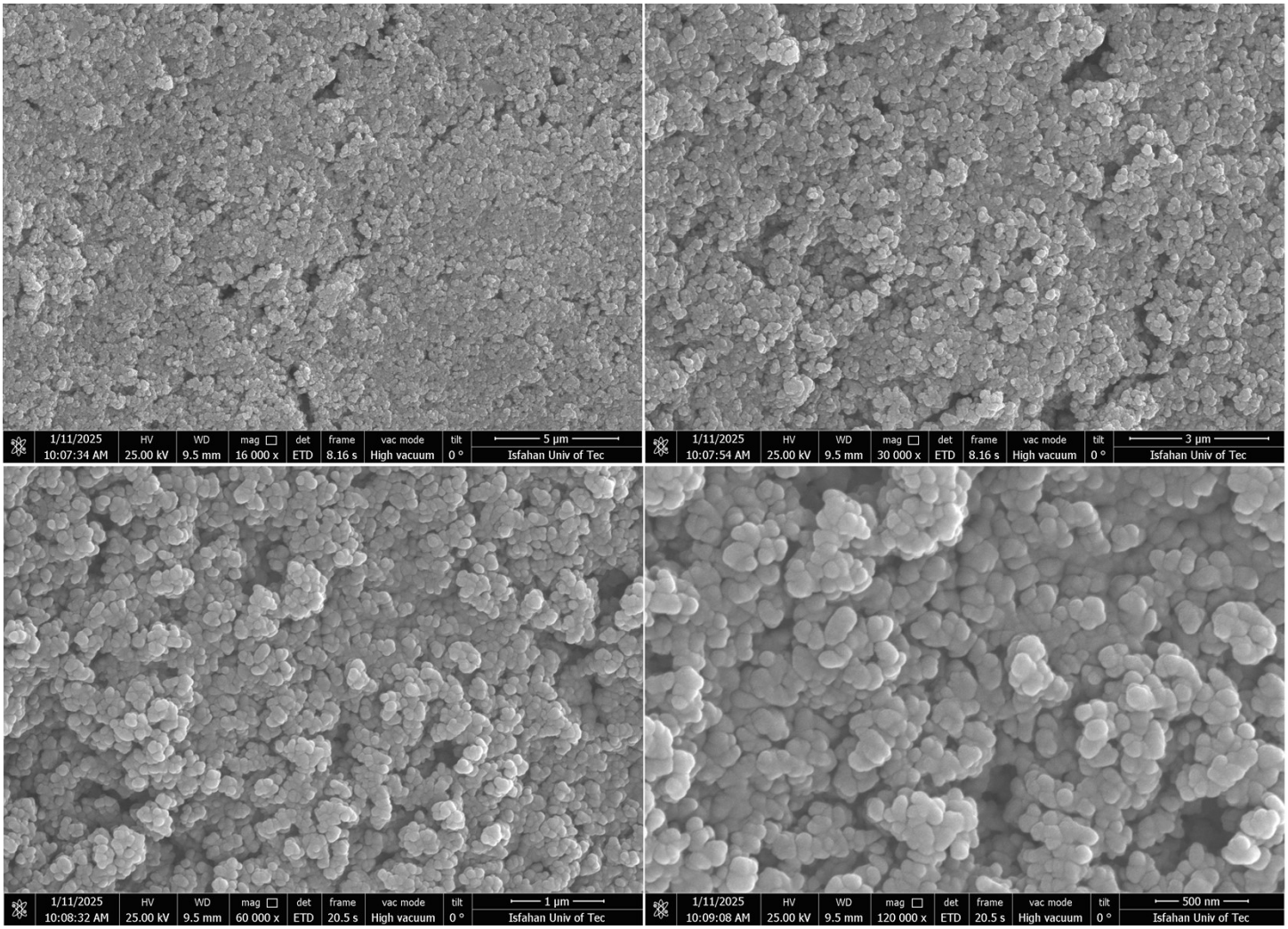

Fig. S6 SEM images, at different magnifications ×16000, ×30000, ×60000, and ×120000 of NF-600 film deposited on the ITO surface.

Supplementary data

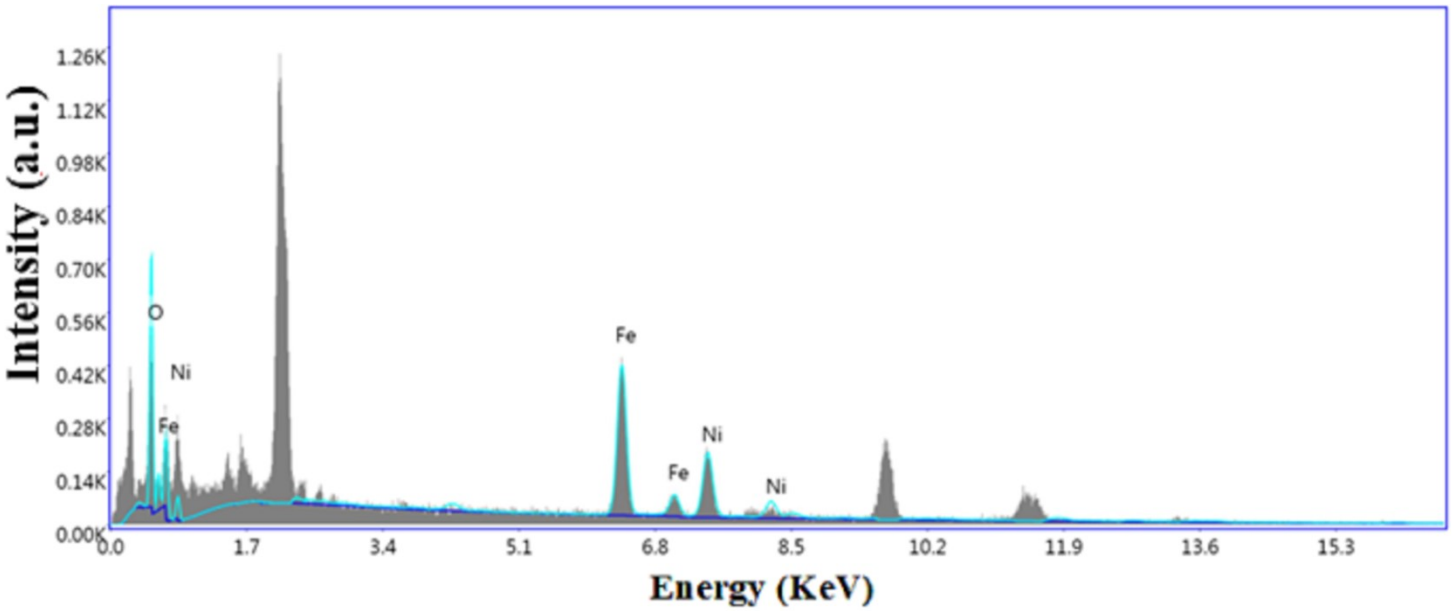

Fig. S7 EDX spectrum of NF-400 sample.

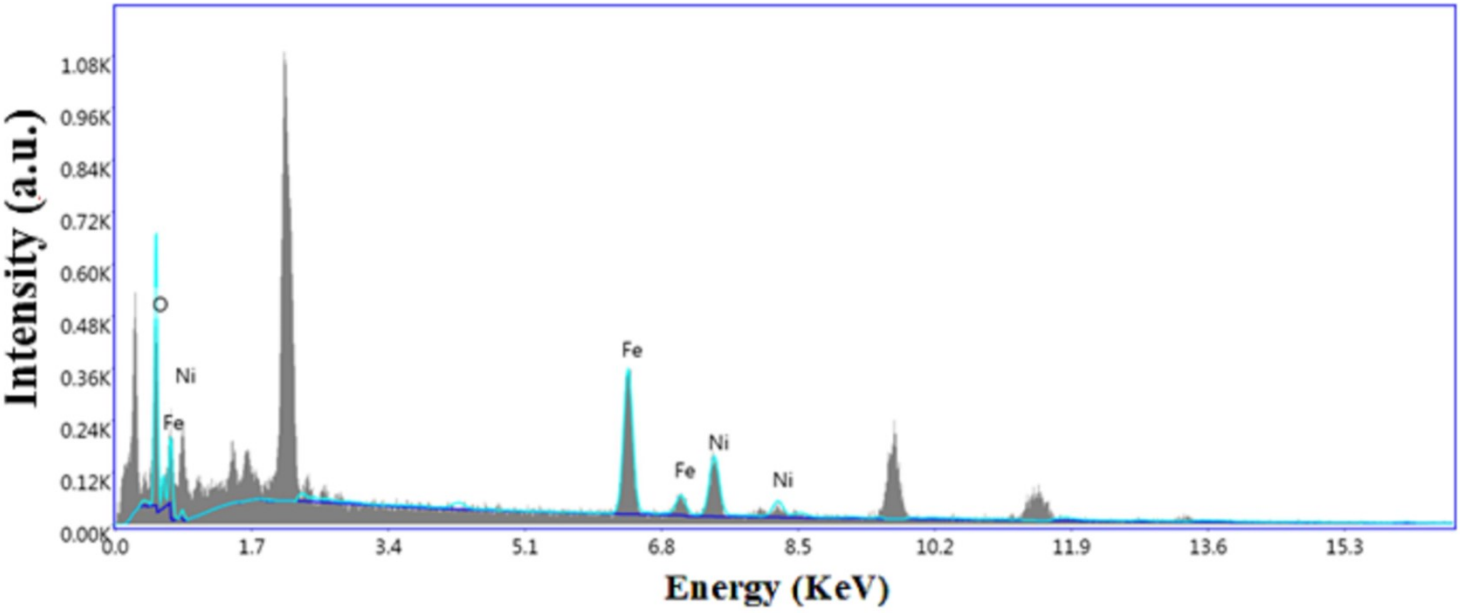

Fig. S8 EDX spectrum of NF-500 sample.

Supplementary data

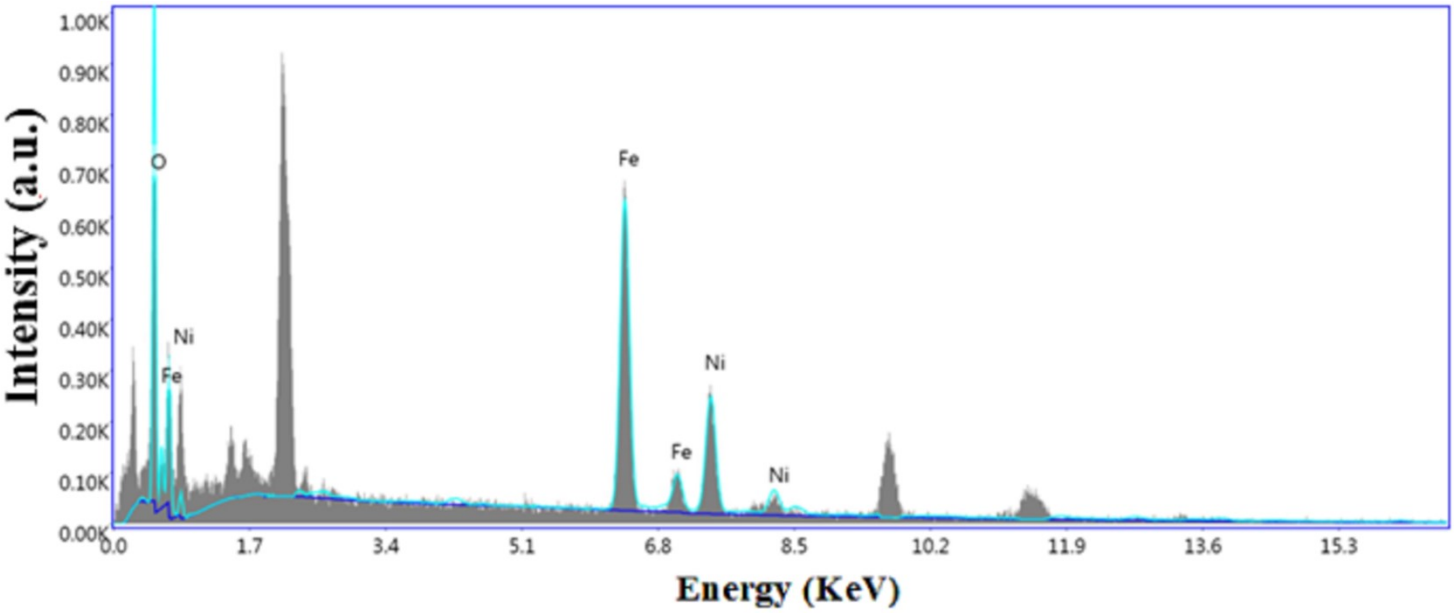

Fig. S9 EDX spectrum of NF-600 sample.

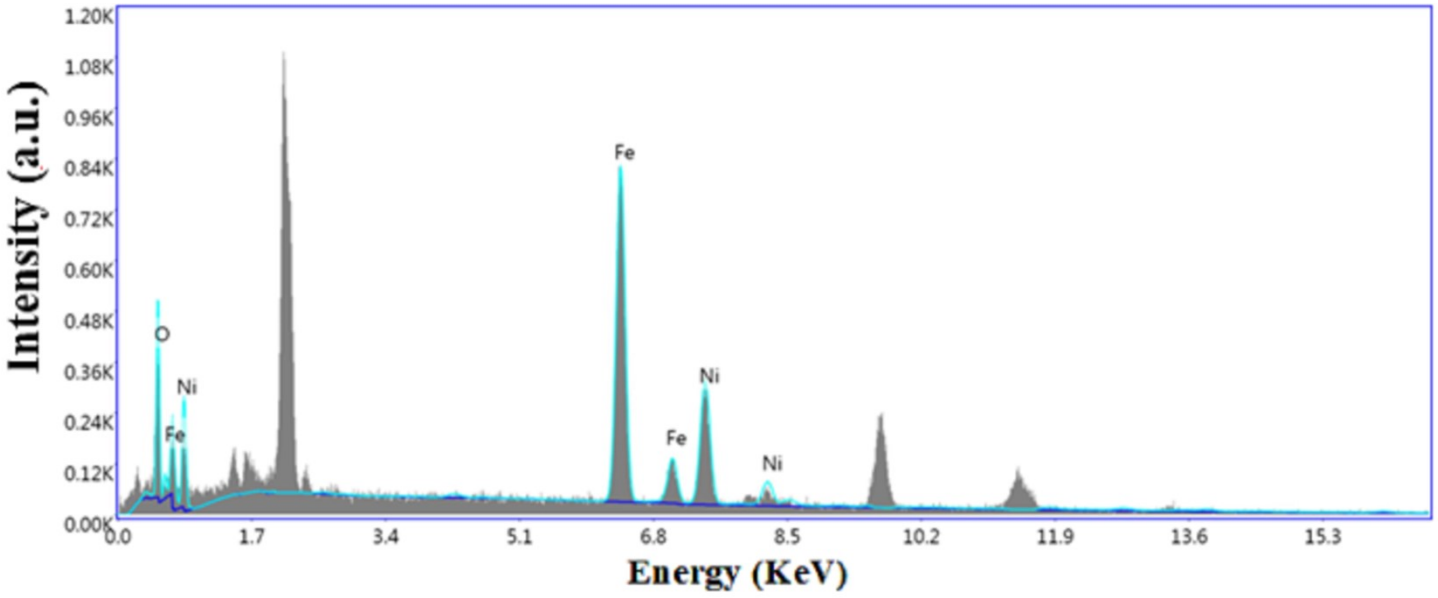

Fig. S10 EDX spectrum of NF-700 sample.

Supplementary data

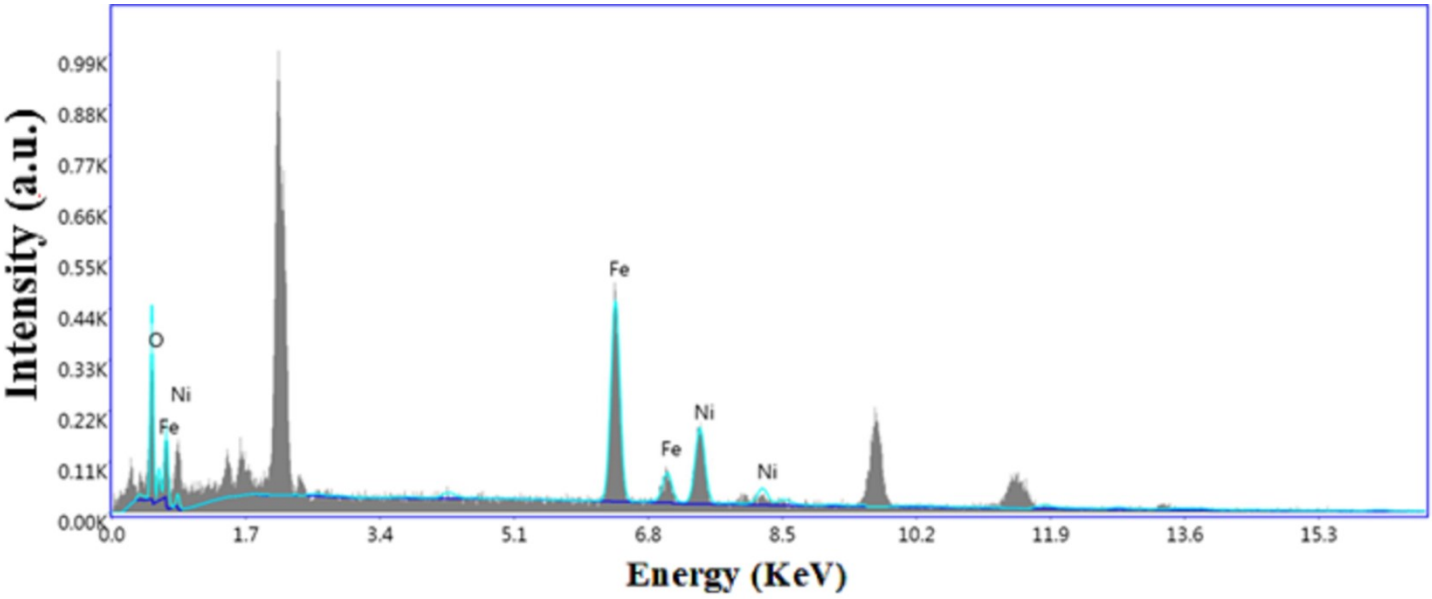

Fig. S11 EDX spectrum of NF-800 sample.

Supplementary data

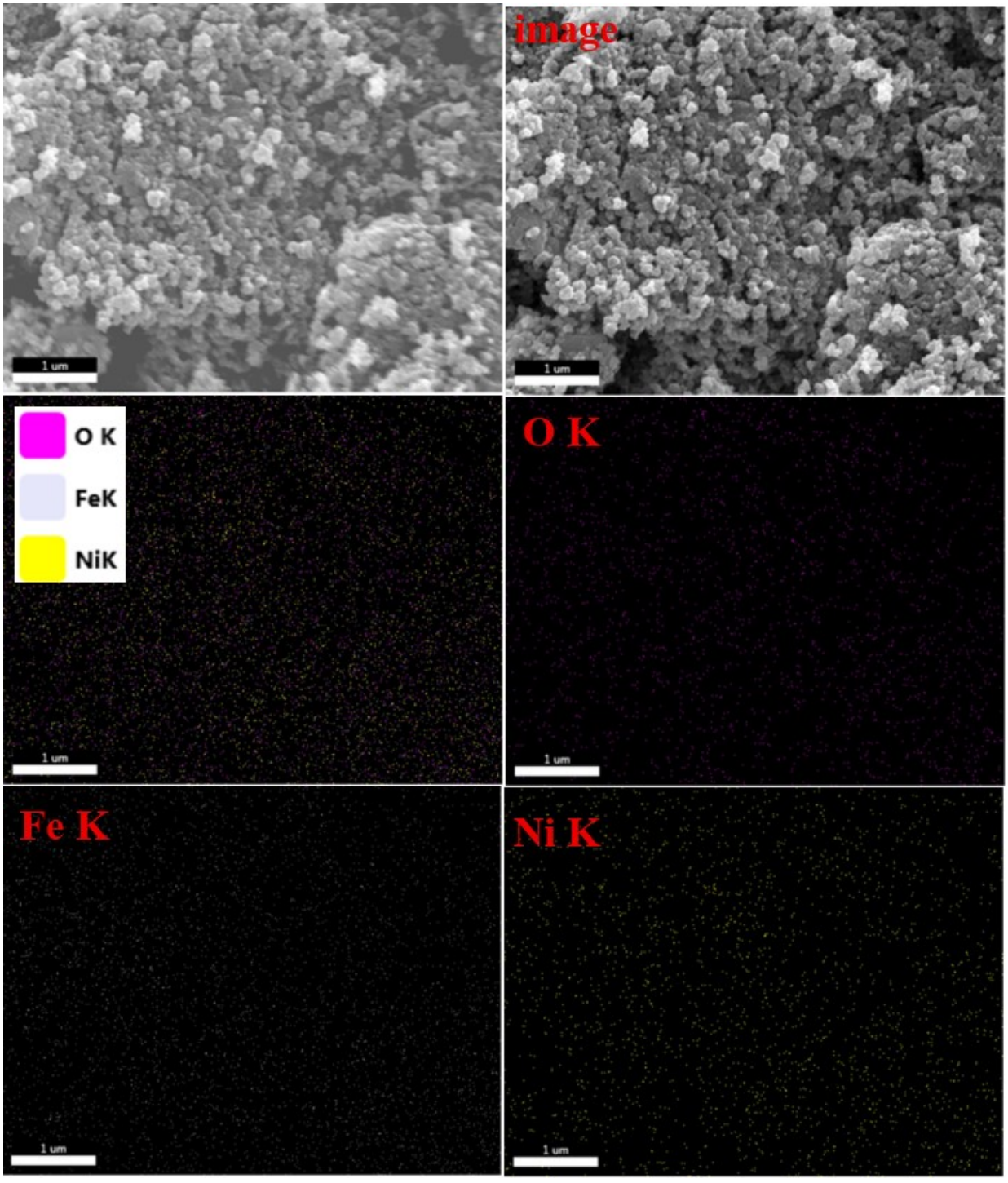

Fig. S12 SEM-EDS elemental mapping of the NF-400 sample.

Supplementary data

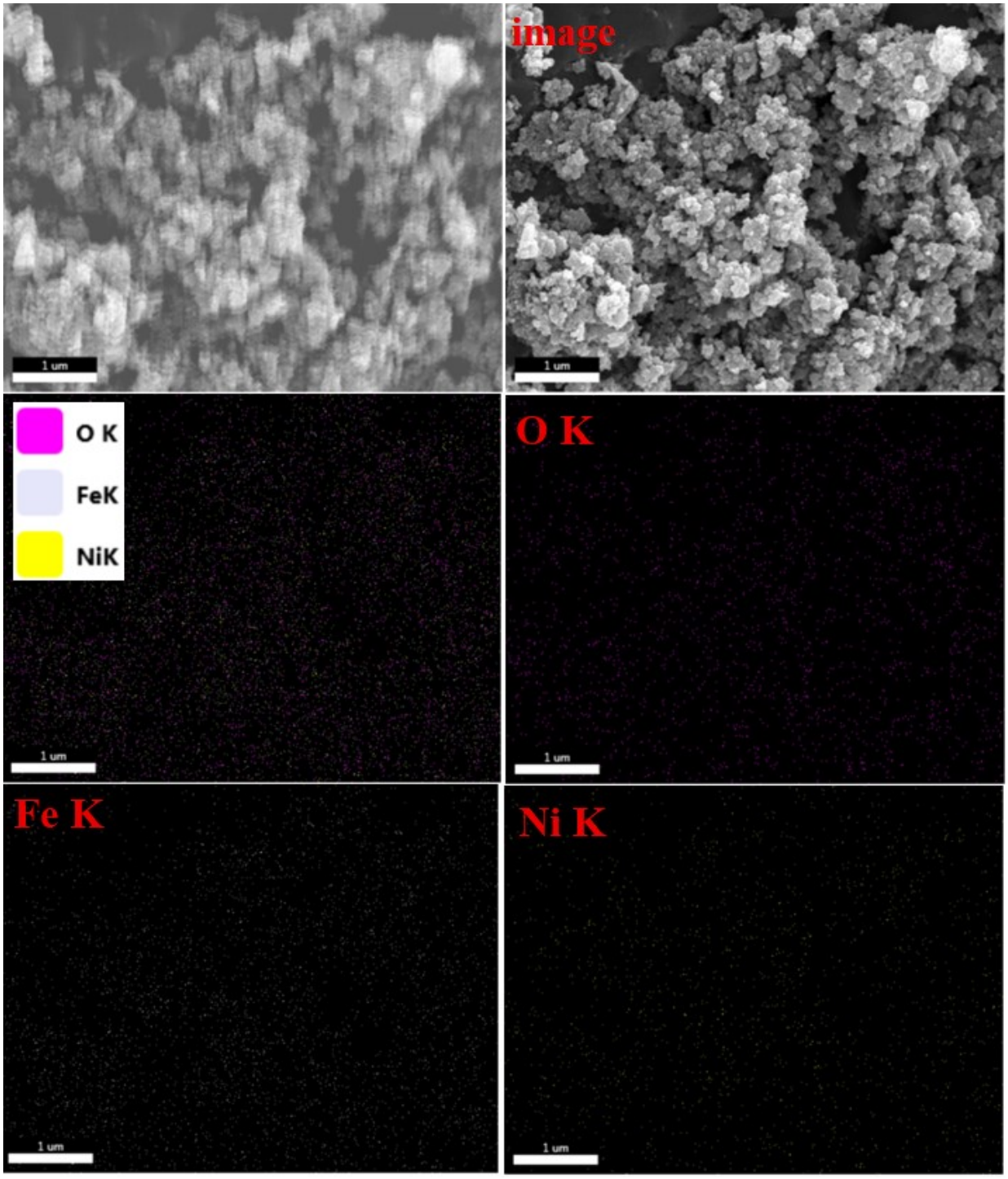

Fig. S13 SEM-EDS elemental mapping of the NF-500 sample.

Supplementary data

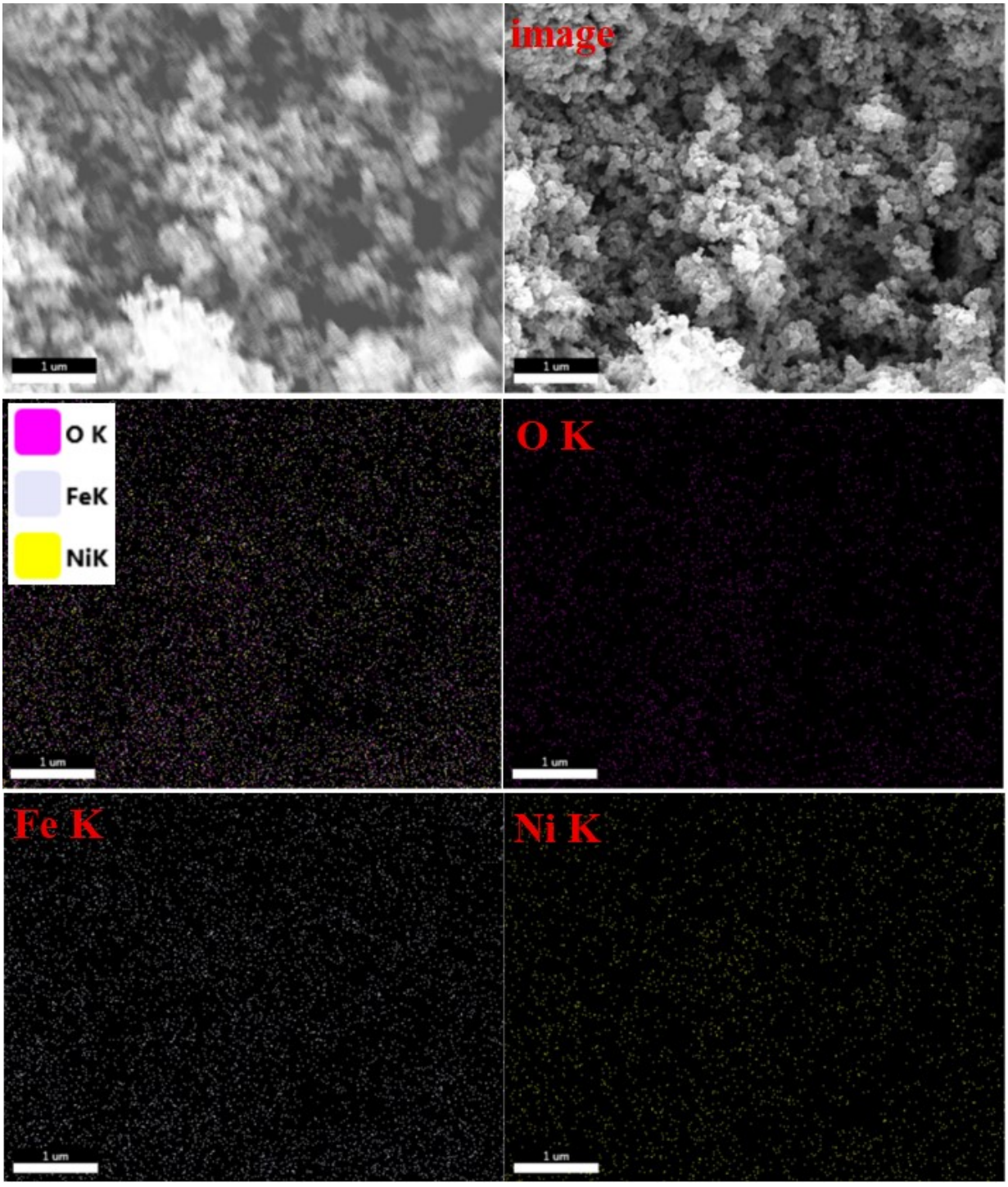

Fig. S14 SEM-EDS elemental mapping of the NF-600 sample.

Supplementary data

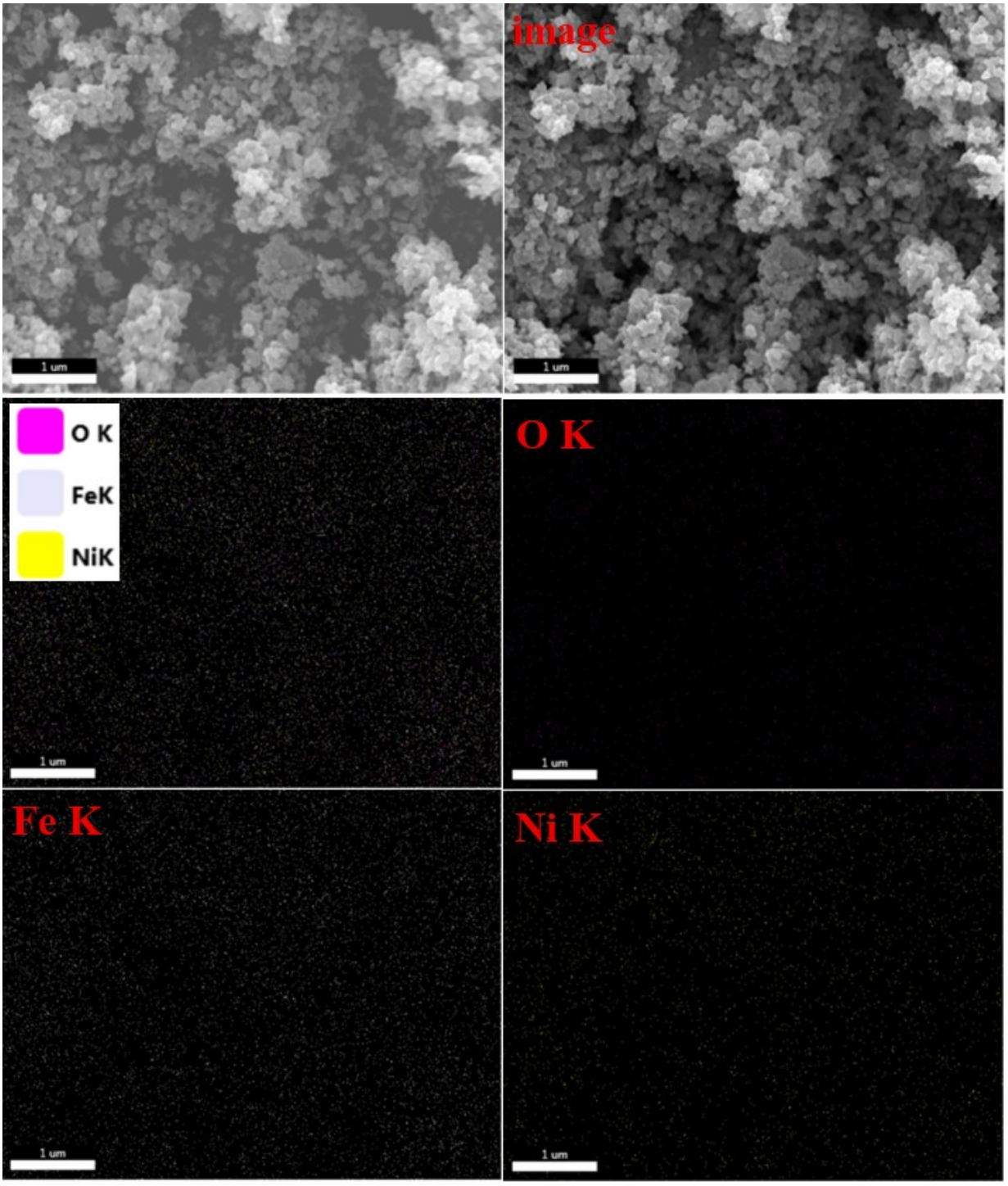

Fig. S15 SEM-EDS elemental mapping of the NF-700 sample.

Supplementary data

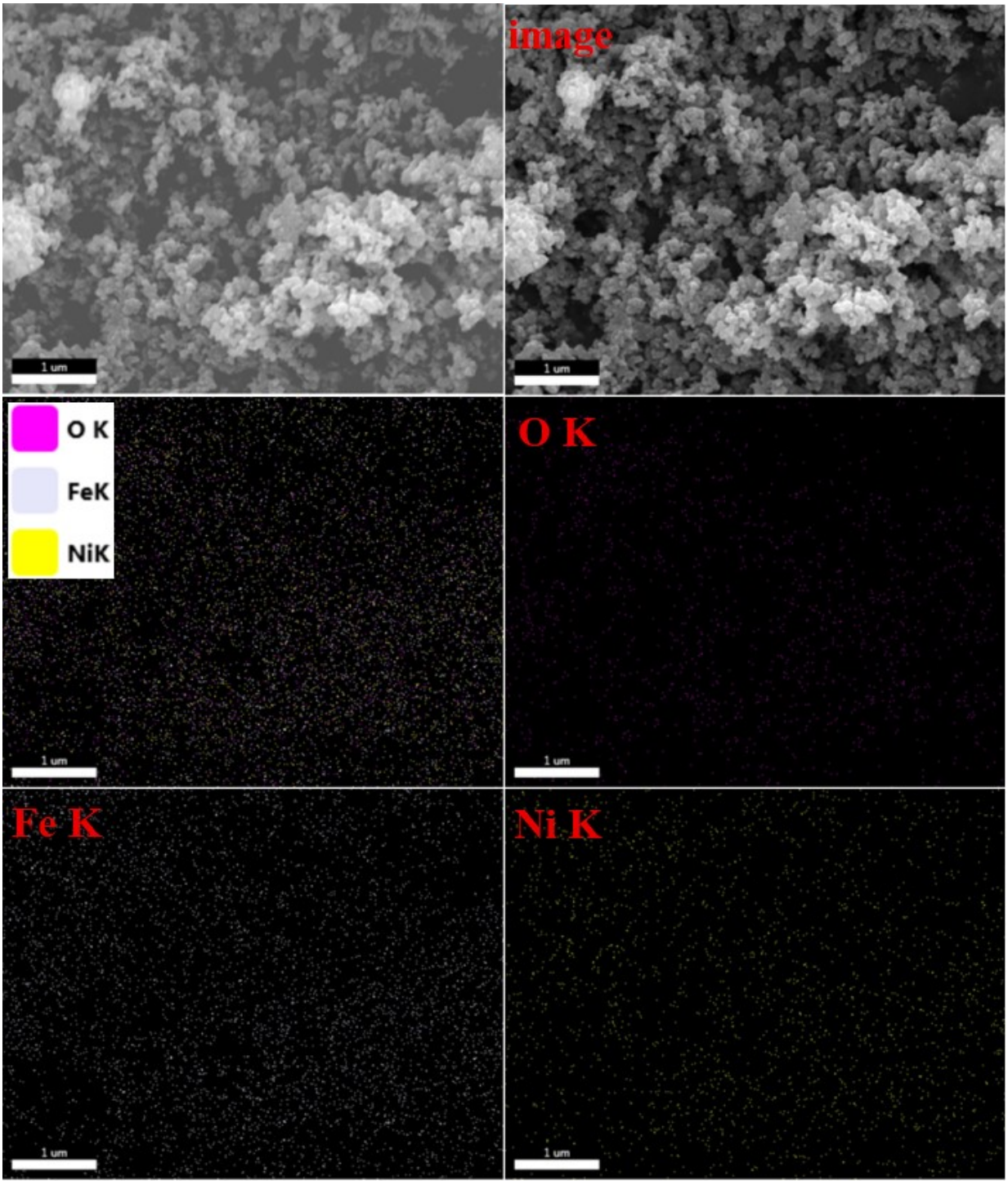

Fig. S16 SEM-EDS elemental mapping of the NF-800 sample.

Supplementary data

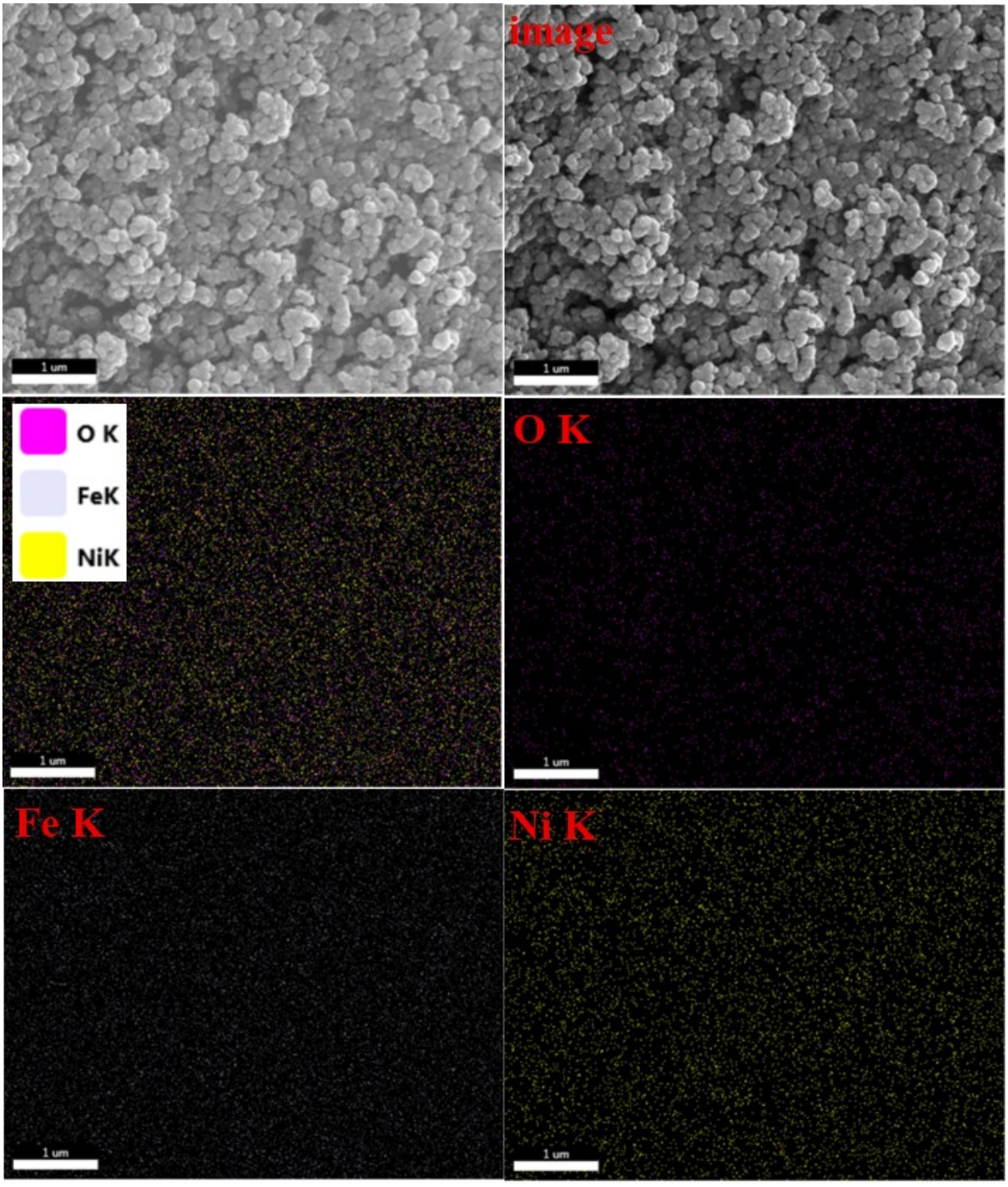

Fig. S17 SEM-EDS elemental mapping of the NF-600 film deposited on the ITO surface.

Supplementary data

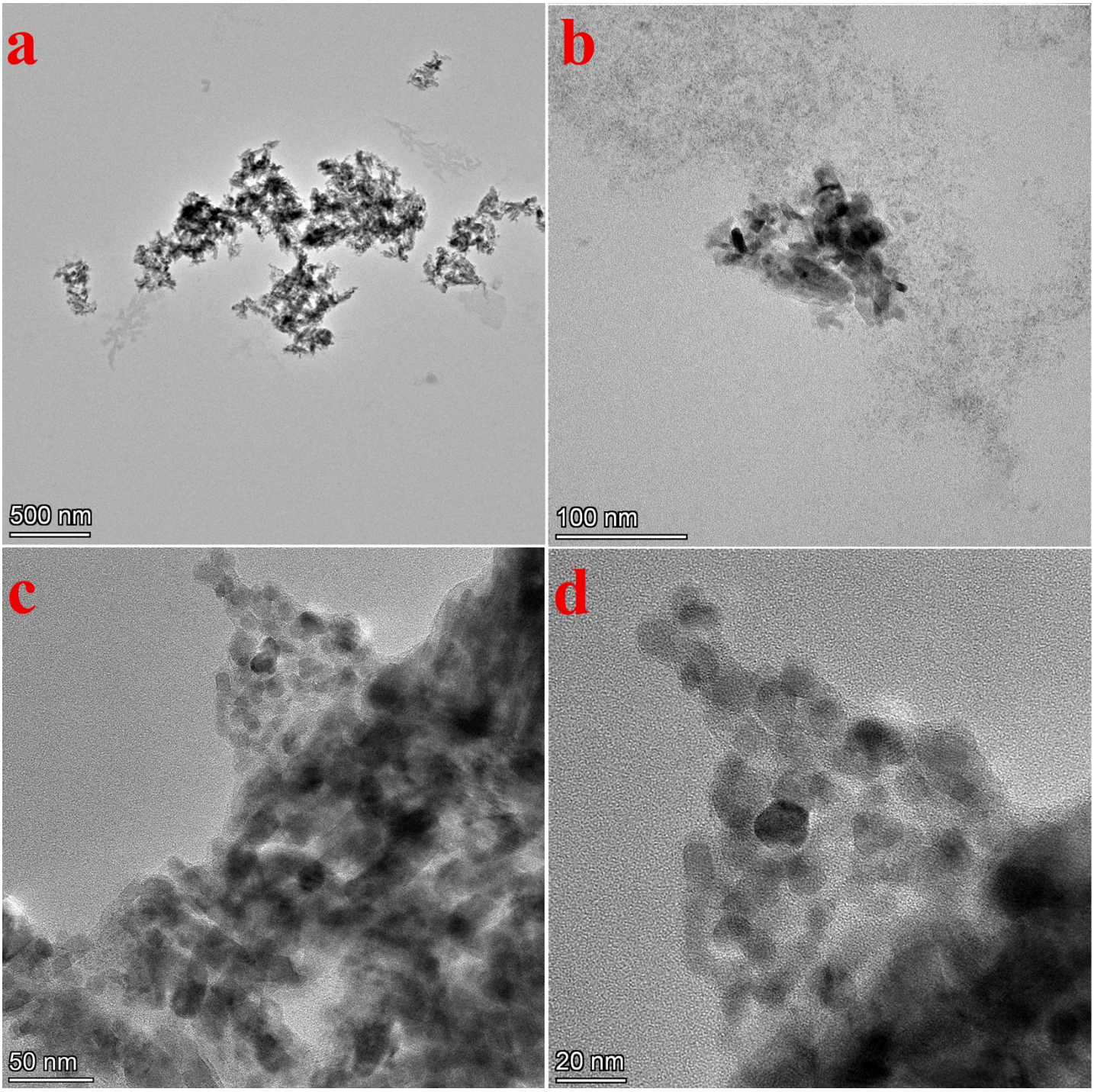

Fig. S18 TEM and HRTEM images obtained at different magnifications of nickel ferrite (sample NF-600).

Supplementary data

Fig. S19 presents the GCD curves of the prepared photoelectrodes with and without light irradiation; all curves exhibit similar shapes. The GCD profiles display typical non-linear charge-discharge behavior, indicating pseudo-capacitive properties that are consistent with the CV curves. Non-linearity and asymmetry in the GCD curves indicate pseudo-capacitive electrode behavior. Comparison of the GCD curves before and after light irradiation shows that the discharge time is extended under illumination, indicating a significant increase in surface capacitance under light. Fig. S19(f and g) compares the GCD curves at a current density of 0.03 mA/cm^2 in the dark and under illumination. The NF-600 electrode exhibits a significantly longer discharge time and therefore a higher capacitance than the other samples (Fig. S20). A capacity of 314.9 mAh/g was determined for the NF-600 sample at 0.03 mA/cm^2, compared to capacities of 146.4, 221.2, 236.8, and 271.8 mAh/g for NF-400, NF-800, NF-700, and NF-500, respectively, confirming that NF-600 is the optimal electrode.[2,3] Fig. S19(h and i) shows the GCD curves for the NF-600 sample at different current densities. Fig. S21 presents the specific capacitance at various current densities under both dark and light irradiation conditions. When illuminated, the capacities range from 422.8 to 222.9 mAh/g at current densities of 0.03 to 0.07 mA/cm^2. In the dark, within the same current density range, the capacities are between 314.9 and 164.7 mAh/g. Exposure to light results in increases in capacitance of 34.2%, 28.3%, 23.6%, 38.7%, and 35.3% at successive current densities (as shown in Fig. S21). A general trend is observed: capacitance increases as current density decreases. At low current densities, electrolyte ions have more time to diffuse into the interior of the distributed pore structure of the nanocomposite electrode, allowing a larger fraction of active sites to participate in charge storage.

Supplementary data

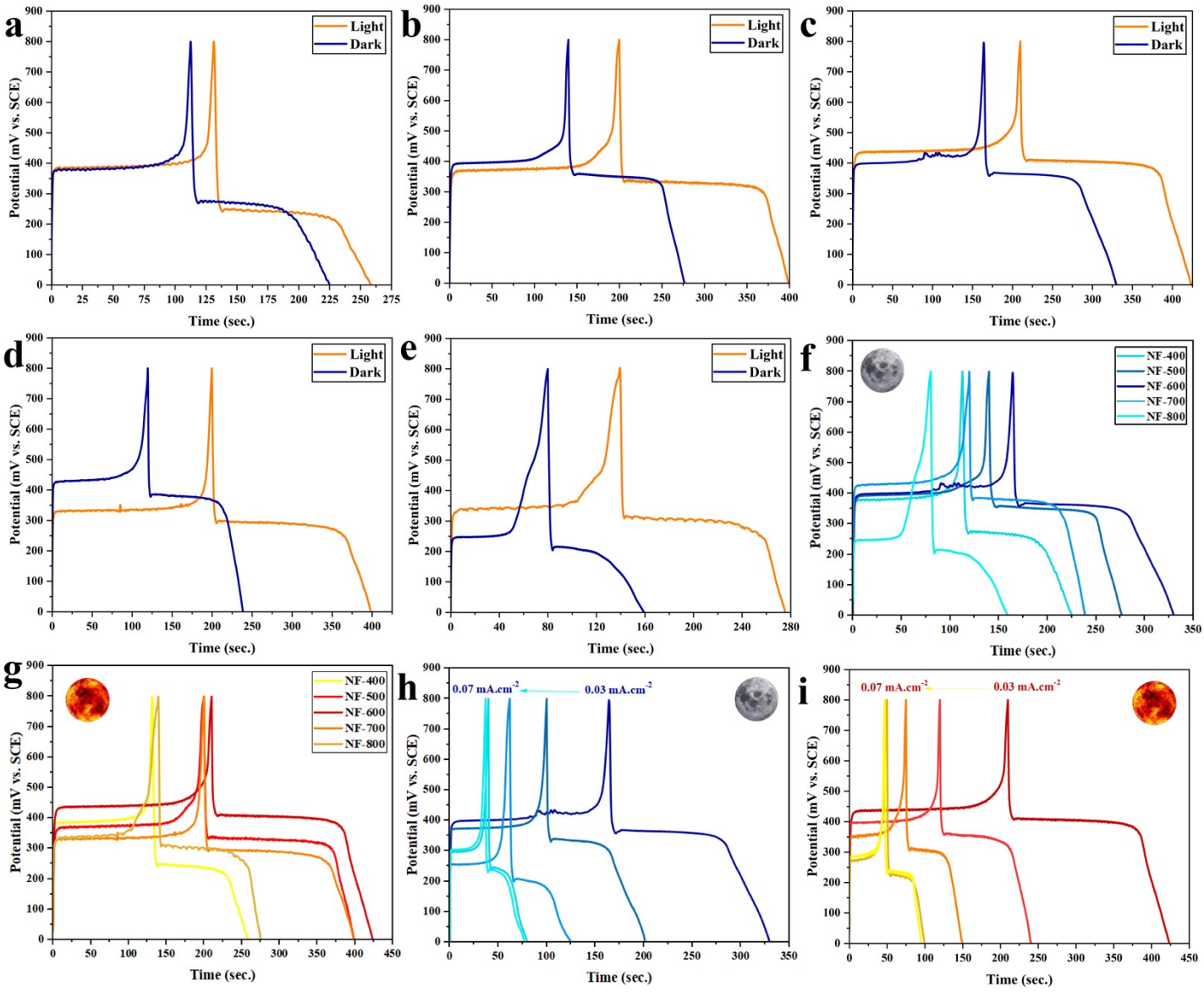

Fig. S19 Comparative GCD plots of different samples at 0.03 mA/cm^2 under dark and light conditions; (a) NF-400, (b) NF-500, (c) NF-600, (d) NF-700, and (e) NF-800. GCD profiles for prepared samples at 0.03 mA/cm^2 (f) in the dark and (g) under light illumination. Charge discharge profile at various current densities for the NF-600 sample (h) in dark and (i) under light conditions.

Supplementary data

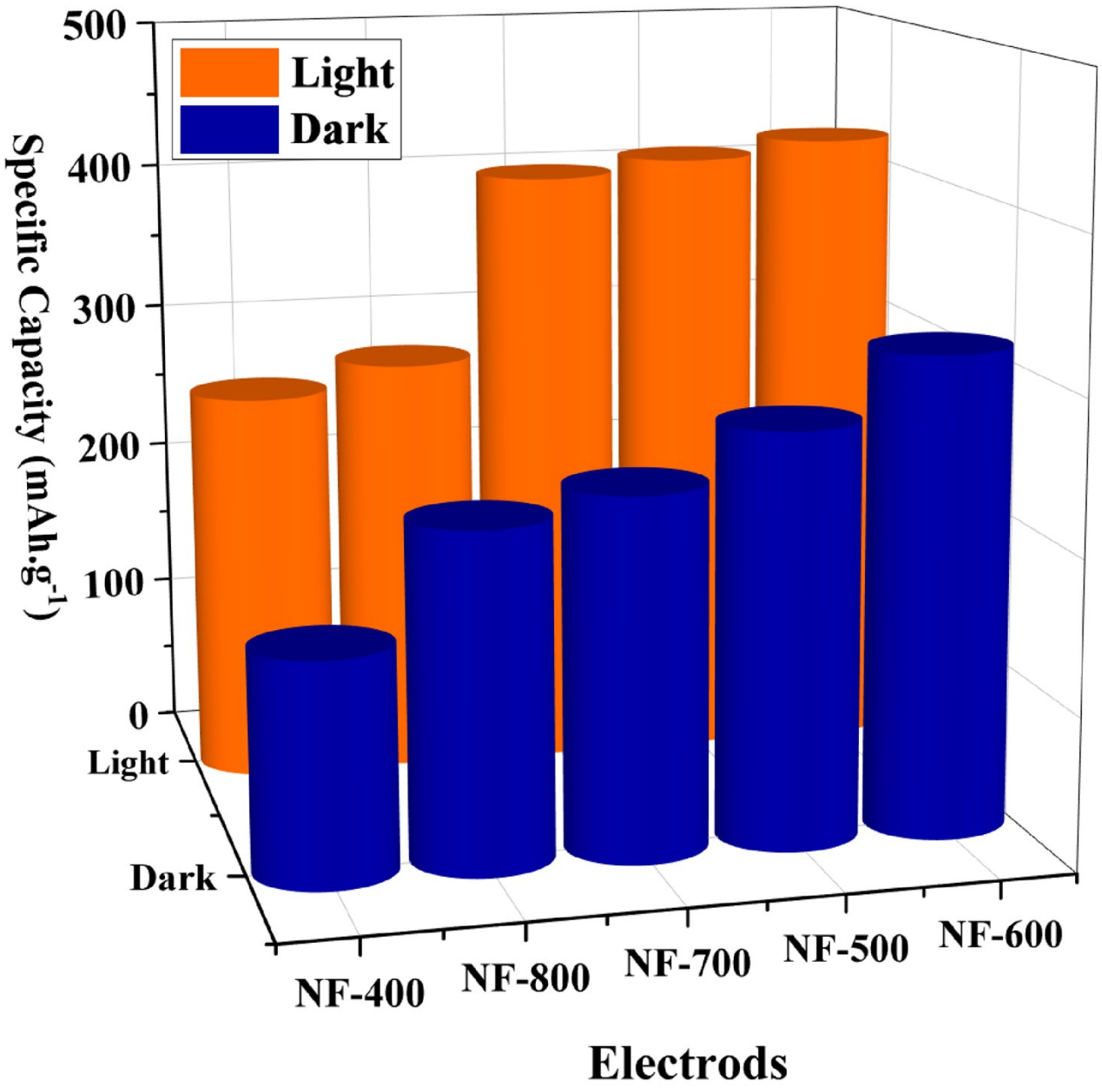

Fig. S20 Histogram plot of the calculated specific capacitance values for different electrodes under both illuminated and dark conditions.

Supplementary data

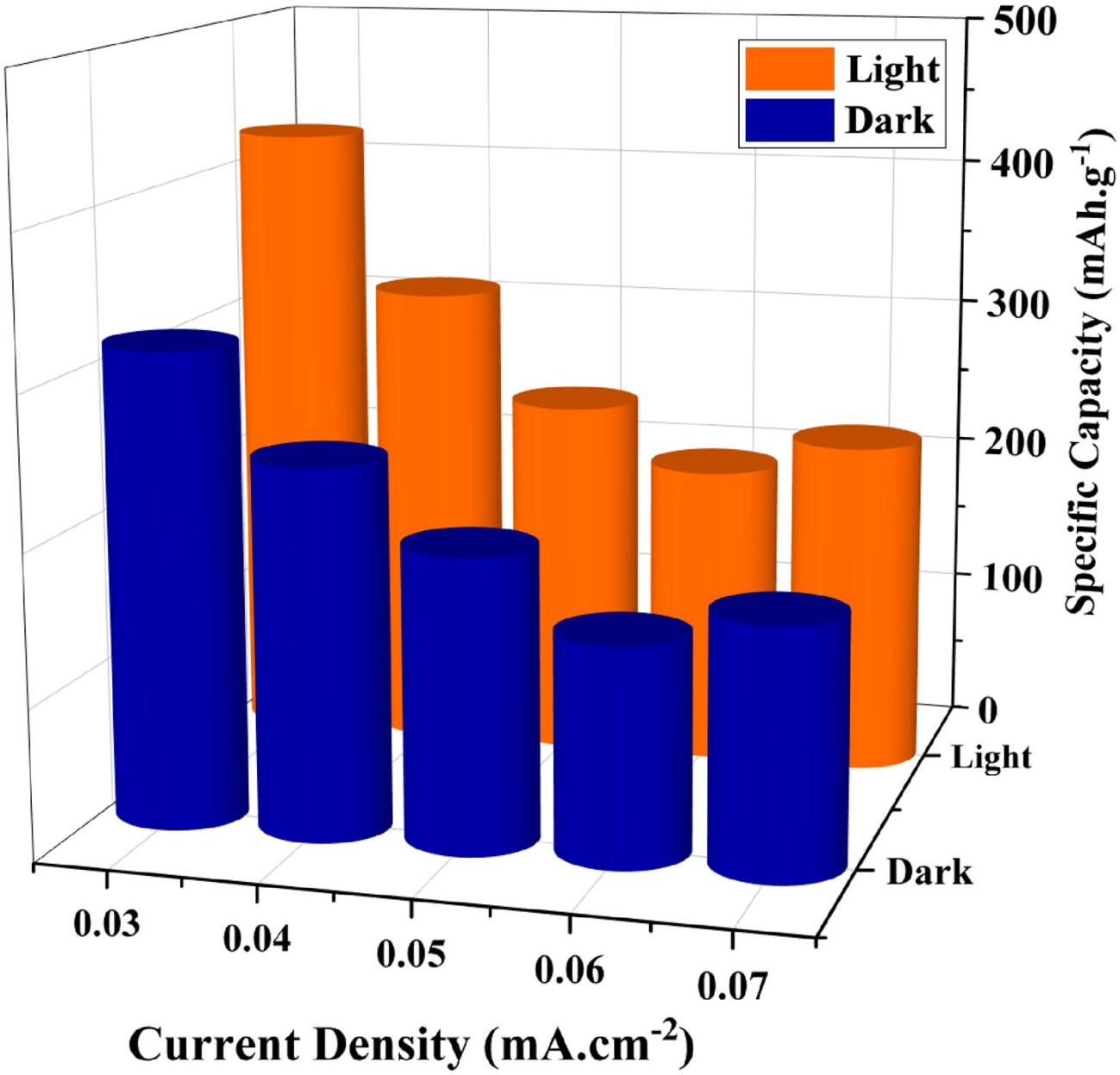

Fig. S21 The plot of specific capacitance at different current densities of the NF-600 sample under both illuminated and dark conditions.

Supplementary data

Capacity enhancement mechanism and structure-performance relationship

To elucidate the origin of the enhanced capacitance of $NiFe_2O_4$ samples under different calcination temperatures and light/dark conditions, a comprehensive structure-performance correlation has been established.

Effect of calcination temperature

XRD and SEM analyses indicate that increasing the calcination temperature from 400 to 600 °C improves the crystallinity and optimizes particle size, reducing grain boundaries and structural defects that can hinder charge transport. Consequently, the NF-600 sample exhibits the highest specific capacitance due to more efficient electron and ion transport. At higher temperatures (>600 °C), particle agglomeration increases, reducing the effective surface area and slightly decreasing the capacitance.

Photo-enhanced capacitance

Under light illumination, the $NiFe_2O_4$ photoelectrodes generate additional electron-hole pairs. These photogenerated carriers enhance charge separation, reduce recombination, and contribute extra faradaic reactions at the electrode/electrolyte interface, resulting in increased capacitance. Chopped chronoamperometry, linear sweep voltammetry, and OCP measurements confirm rapid and reversible photocurrent responses corresponding to light ON/OFF cycles (Figs. S21-S23). Therefore, a clear correlation between the structural characteristics and electrochemical performance can be established. An optimal (moderate) calcination temperature provides a balanced combination of appropriate crystallinity and sufficient surface defects, resulting in maximum capacitance. In contrast, further increasing the temperature leads to grain growth and a reduction in specific surface area, which

consequently decreases the capacitance. Moreover, under light illumination, additional photo-induced charge carriers are generated, contributing to enhanced capacitance compared to dark conditions.

Open-Circuit Potential (OCP):

OCP measurements were conducted under dark and illuminated conditions (Figure S21). Upon light irradiation, a clear shift of potential was observed, indicating effective photo-generated charge separation and band bending modification.

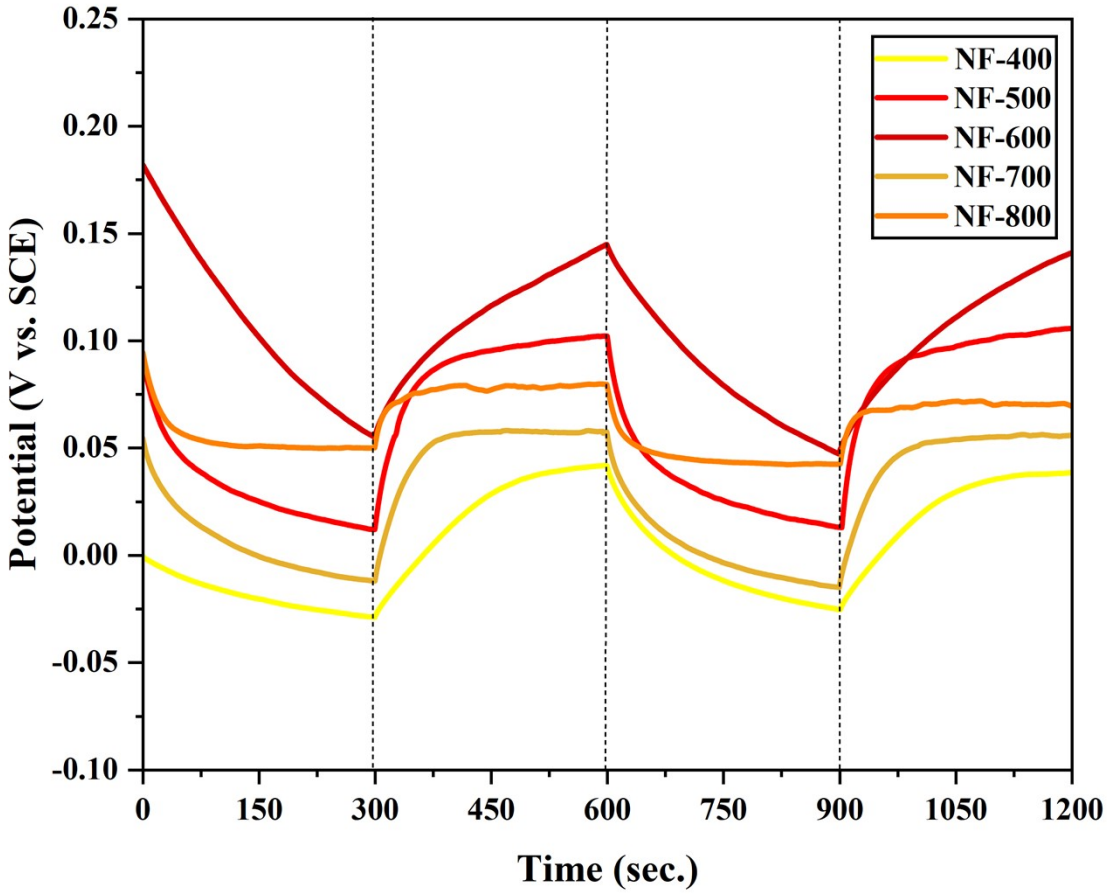

Fig. S22 Illuminated Open-Circuit Potential (OCP) versus time under off/on cycles of light illumination of different $NiFe_2O_4$ photoelectrodes vs SCE reference.

Supplementary data

Chopped Chronoamperometry (CA):

The transient photocurrent response was investigated using chopped light illumination. The electrodes exhibited rapid and reproducible current responses upon light ON/OFF cycles, confirming stable and reversible photo-induced charge transfer.

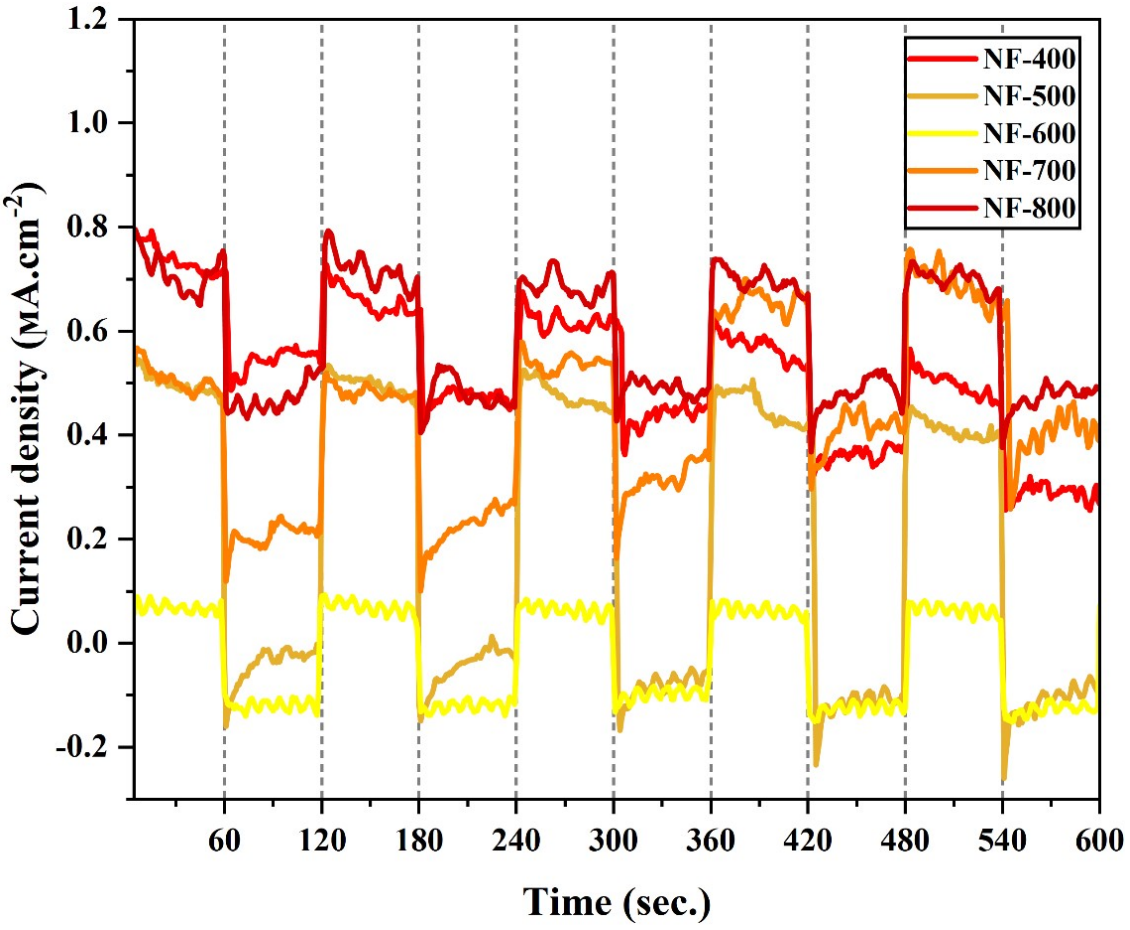

Fig. S23 Chopped light chronoamperometry experiments of different $NiFe_2O_4$ photoelectrodes.

Supplementary data

Chopped Linear Sweep Voltammetry (LSV):

Chopped LSV curves were recorded to examine the influence of illumination on electrochemical behavior (Figure S23). A significant enhancement in current density under illumination was observed across the potential range, confirming improved photoelectrochemical kinetics.

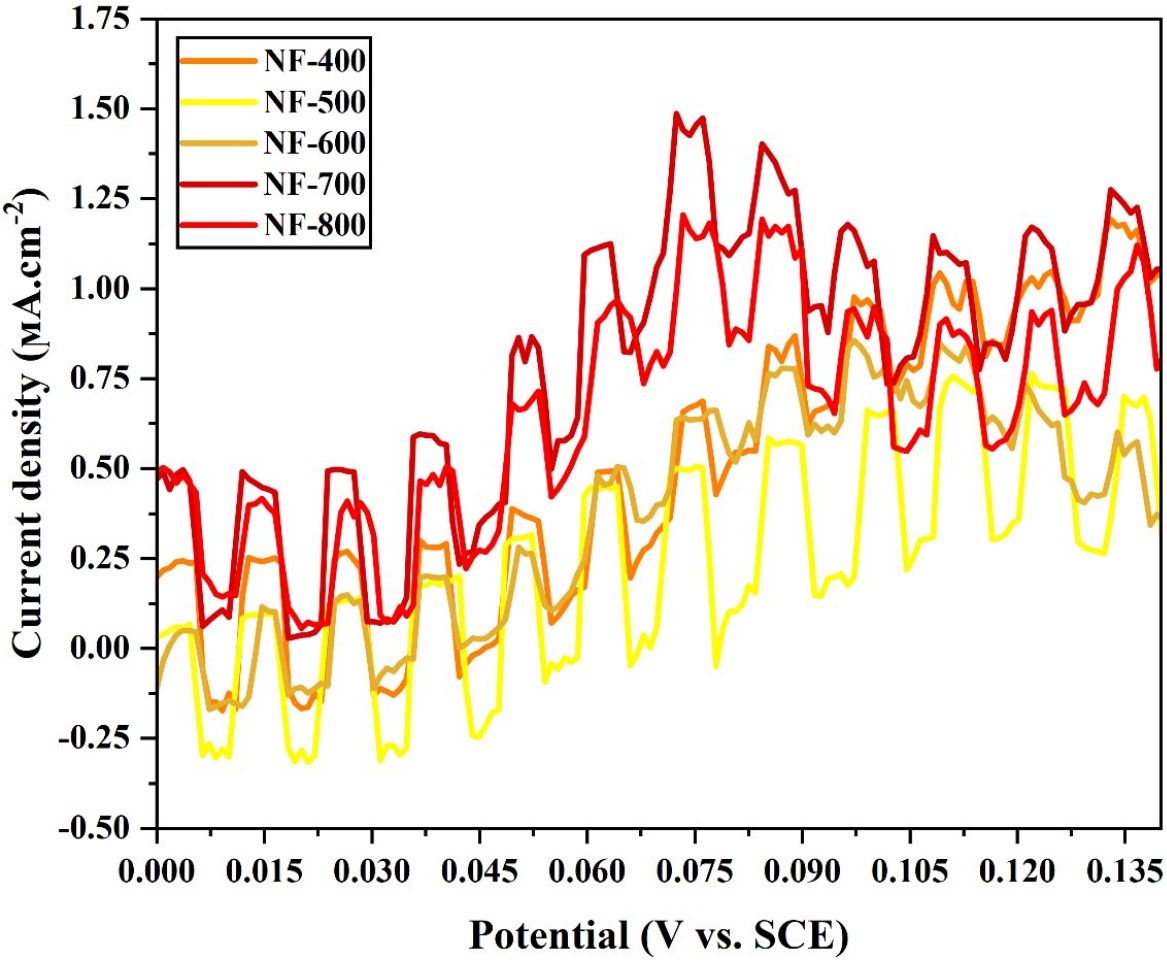

Fig. S24 Chopped linear sweep voltammetry (LSV) curves of different $NiFe_2O_4$ photoelectrodes.

Supplementary data

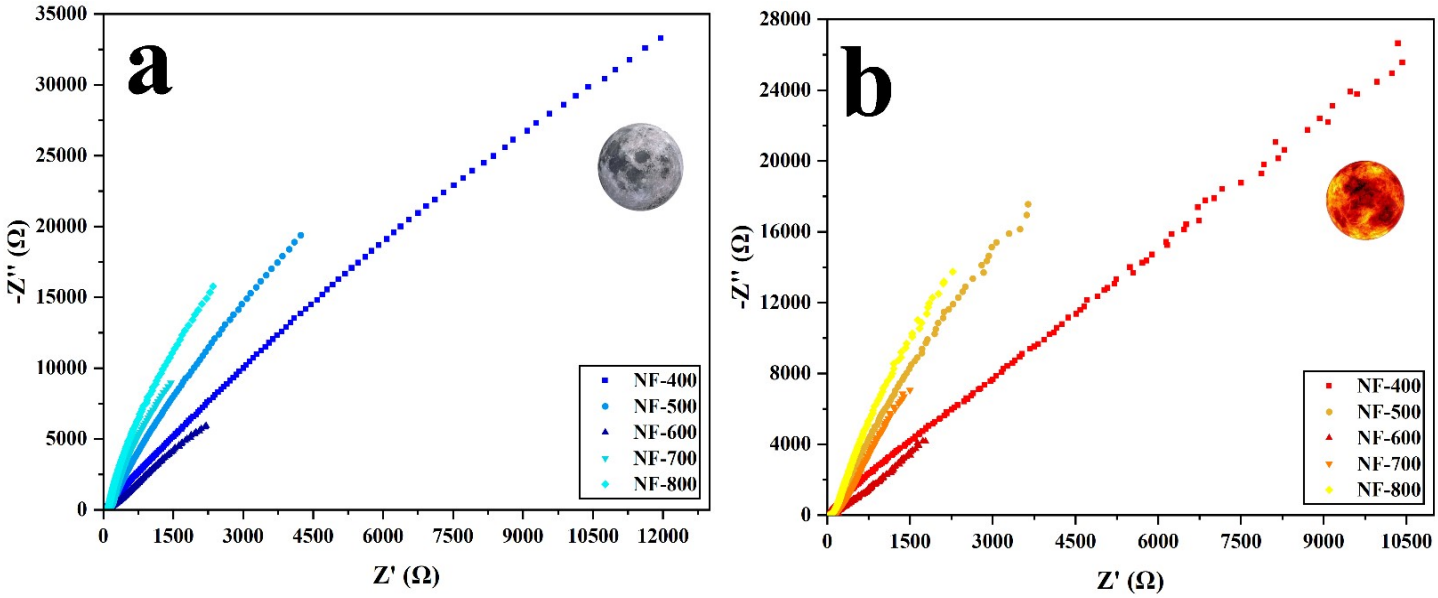

Fig. S25 EIS diagrams of different electrodes (a) in the dark and (b) under light irradiation.

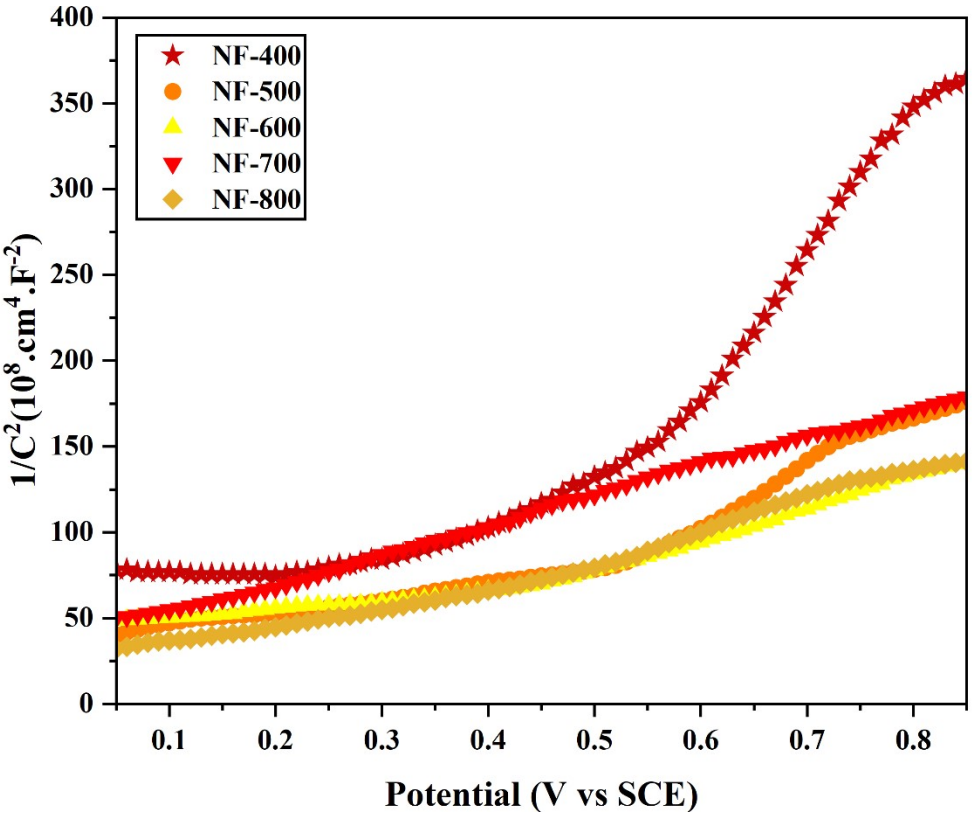

Fig. S26 Mott-Schottky plots measured in the dark at 1 kHz frequency for different NiFe2O4-based electrodes

Supplementary data

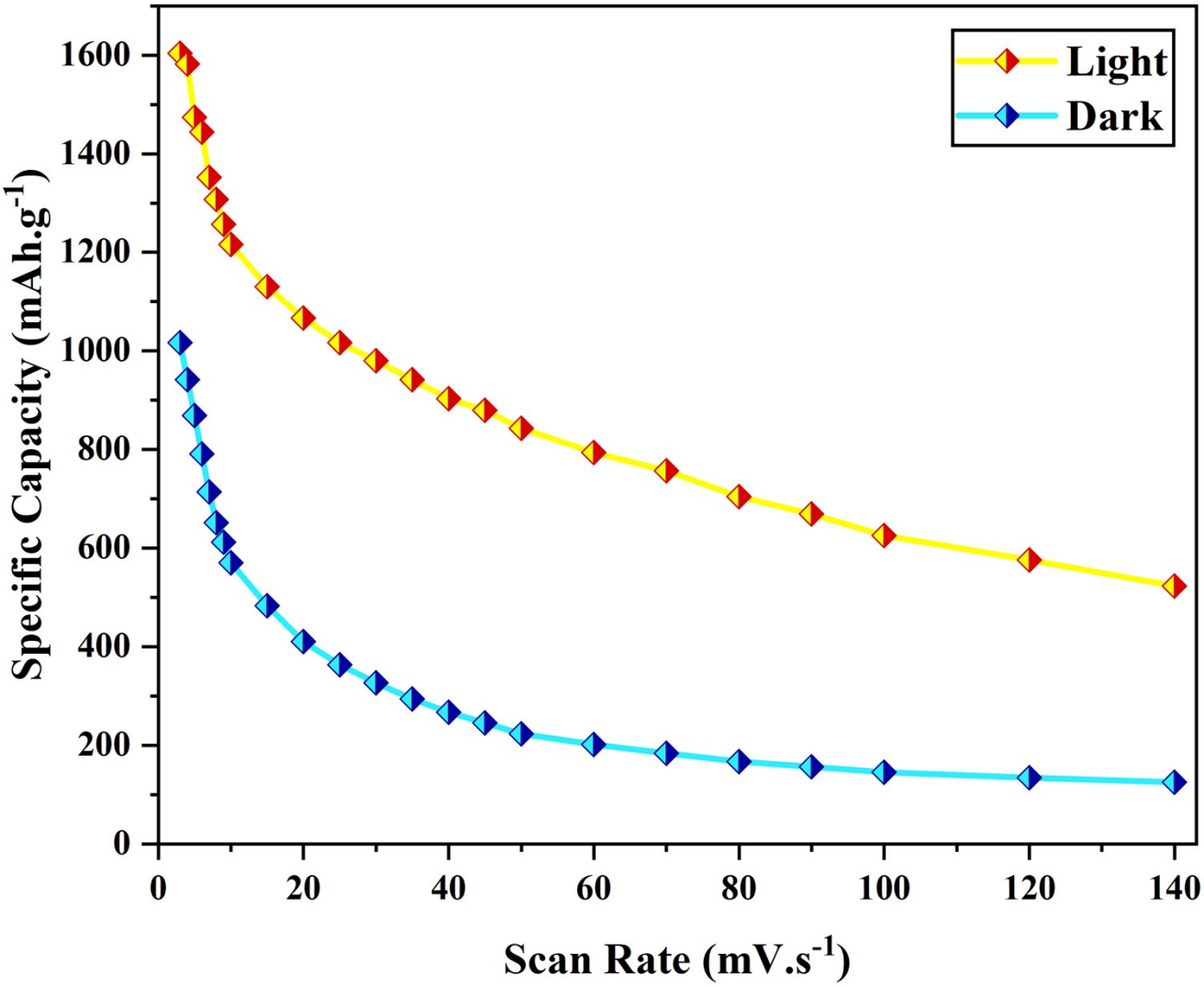

Fig. S27 Capacitance vs. scan rate curves based on CV data for the asymmetric flexible photo-powered supercapacitor (AFPPSC) under illuminated and dark conditions.

Supplementary data

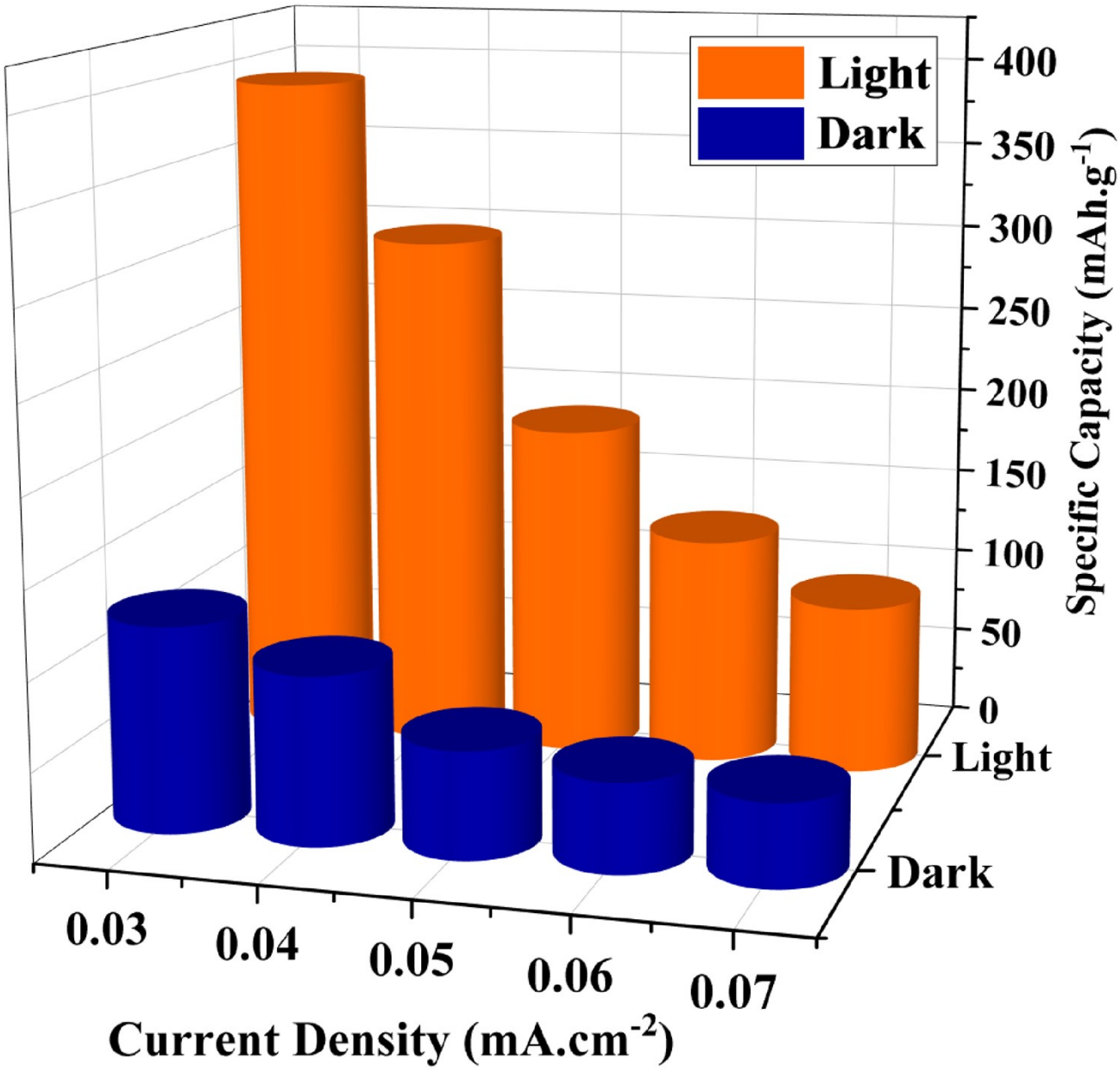

Fig. S28 The plot of specific capacitance at different current densities for the asymmetric flexible photo-powered supercapacitor (AFPPSC) under both illuminated and dark conditions.

Supplementary data

Table S1. Extracted fitting parameters obtained from the equivalent electrical circuit (EEC) model for the NF-400, NF-500, NF-600, NF-700, and NF-800 samples under light and dark conditions.

	Sample	R_1 (Ω)	R_2 (Ω)	CPE_1-T (mF/cm^2s^{n-1})	CPE_1-P (mF/cm^2s^{n-1})	R_3 (Ω)	CPE_2-T (mF/cm^2s^{n-1})	CPE_2-P (mF/cm^2s^{n-1})	χ^2
Light	NF-400	38.14	204500	0.000045809	0.81167	124.9	0.00013485	1.399	0.0037085
	NF-500	57.03	123330	0.0010475	0.4633	100630	0.000090436	0.98859	0.00085985
	NF-600	22.17	3448400	0.00074681	0.4908	$1.04*10^{11}$	0.00047362	0.89908	0.044234
	NF-700	72.82	$9.9994*10^{19}$	0.0023578	0.32542	$1.0003*10^{20}$	0.00021558	0.93352	0.0019665
	NF-800	27.34	$1.0491*10^{20}$	0.0013597	0.43442	145670	0.00011881	0.98747	0.0026305
Dark	NF-400	36.49	382120	0.00003848	0.83272	2.403	0.0000019397	1.045	0.00066264
	NF-500	87.83	117.4	0.00053912	0.54015	143430	0.000075914	0.9406	0.00095576
	NF-600	22.06	$1*10^{20}$	0.00045292	0.55953	30988	0.00039307	1.45	0.0021471
	NF-700	78.74	$1*10^{20}$	0.0020218	0.3389	48577	0.00017561	1.038	0.0016467
	NF-800	27.79	$9.9922*10^{19}$	0.001204	0.44514	70545	0.000099922	1.047	0.0042661

Table S2. Extracted fitting parameters obtained from the equivalent electrical circuit (EEC) model for the asymmetric (AFPPSC) and symmetric (SPPSC) photo-powered supercapacitors under light and dark conditions.

	Sample	R_1 (Ω)	R_2 (Ω)	CPE_1-T (mF/cm^2s^{n-1})	CPE_1-P (mF/cm^2s^{n-1})	R_3 (Ω)	CPE_2-T (mF/cm^2s^{n-1})	CPE_2-P (mF/cm^2s^{n-1})	χ^2
AFPPSC	Light	20.3	1310	0.001935	0.45689	19522	0.00021804	0.92404	0.00043493
	Dark	16.65	24.7	0.0017735	0.51529	46819	0.00006086	0.87385	0.0002145
SPPSC	Light	50.92	69.27	0.00013975	0.70556	36925	0.00028327	0.83255	0.0010496
	Dark	43.61	31346	0.0010123	0.45204	15078	0.00033174	1.061	0.0030902